Electric field control of magnetization reversal in FeGa/PMN-PT thin films

JPhys Materials

PURPOSE-LED PUBLISHING™

PAPER • OPEN ACCESS

Electric field control of magnetization reversal in FeGa/PMN-PT thin films

To cite this article: Gajanan Pradhan *et al* 2024 *J. Phys. Mater.* **7** 015016

IOP Publishing J. Phys. Mater. 7 (2024) 015016 https://doi.org/10.1088/2515-7639/ad1e13

Journal of Physics: Materials

OPEN ACCESS

RECEIVED
31 May 2023

REVISED
1 January 2024

ACCEPTED FOR PUBLICATION
12 January 2024

PUBLISHED
25 January 2024

PAPER

Electric field control of magnetization reversal in FeGa/PMN-PT thin films

Gajanan Pradhan[1,2,*], Federica Celegato[1], Alessandro Magni[1], Marco Coisson[1], Gabriele Barrera[1], Paola Rizzi[2] and Paola Tiberto[1]

[1] Advanced Materials and Life Science Divisions, Istituto Nazionale di Ricerca Metrologica (INRIM), Strada delle Cacce 91, Turin 10135, Italy
[2] Chemistry Department and NIS, University of Turin, via Pietro Giuria 7, Turin 10125, Italy
* Author to whom any correspondence should be addressed.

E-mail: g.pradhan@inrim.it

Keywords: magnetoelectric effect, magnetic domain, strain, magneto-optic Kerr effect

Abstract

Artificial magnetoelectric materials possess huge potential to be utilized in the development of energy efficient spintronic devices. In the past decade, the search for a good ferromagnetic/ferroelectric combination having the ability to create high magnetoelectric coupling, created new insights and also new challenges. In this report, the magnetoelectric effect is studied in the FeGa/PMN-PT(001) multiferroic heterostructures in the presence of electric fields via strain-mediated effects. The formation of magnetic anisotropy in FeGa is observed after changing the polarization of PMN-PT to out-of-plane orientations. The magnetic domain structures forming during the magnetization reversal were studied in compressive, tensile and remanent strained states. The changes in the magnetic properties were reversible after each cycling of the electric field polarity, hence creating a non-volatile system. The control of magnetization switching sustained by an ON–OFF electric field makes our multiferroic heterostructure suitable for application in low-power magnetoelectric based memory applications.

1. Introduction

The manipulation of magnetic properties with the sole use of electric field has attracted new attention in recent years for its potential ability in low power memories and solid-state devices [1–5]. A major advantage over conventional storage devices is reducing the amount of energy required to flip the magnetization during data writing. In this context, multiferroic materials are suitable candidates having more than one ferroic order and typically show an interplay between ferromagnetism and ferroelectric behavior [6–12]. However, the ordering temperatures of these materials are low, which limits their usage for room-temperature devices [13, 14]. Artificial multiferroics play a major role in this aspect, where different combinations of magnetic layers can be stacked on a piezoelectric substrate [15–20]. The application of an electric field induces deformation in the piezoelectric layer via the inverse piezoelectric effect. The strain is transferred at the interface to the magnetic layer that modifies the magnetic anisotropy and domain structures. Materials possessing high magnetostriction are ideal to generate more control over magnetization changes through strain effects as compared to other ferromagnets. Another method of influencing the magnetization is by inducing migration of ions from an oxide to using an electric field creating a significant change in magnetization [21–23]. However, the reversibility is compromised by a volatile behavior after repeated switching.

A good piezoelectric substrate with high piezoelectric coefficients along with a highly magnetostrictive material can be a promising combination to enhance the effect of strain effect on magnetization. Among the available piezoelectric materials, relaxor ferroelectric $Pb(Mg_{1/3}Nb_{2/3})O_3$-$PbTiO_3$(PMN-PT) has high piezoelectric constants [24–26]. With a PT concentration of 30%–40%, the material lies in a morphotropic

phase boundary and consists of a mixed phase of rhombohedral and tetragonal phases [27–29]. Several works have been performed with this substrate involving different ferromagnetic materials like Co [30], FePt [31], FeSi [32], FeCoSiB [33], etc, where the effect of strain on the change in anisotropy has been studied. Various in-plane strained states can be stabilized at remanence by cycling controllably the electric field applied through the thickness of the PMN-PT [34]. This can be effectively used to control the magnetic domains [35–37]. In the case of PMN-PT(001), the spontaneous polarization lies long the <111> directions (out-of-plane). With the application of opposite electric field, the polarization switches in-plane via 109° switching thereby generating in-plane strains and permitting non-volatile magnetoelectric effects [38, 39].

Strain induction by electric field also results in the formation of surface cracks, which might result in a discontinuity in the magnetic thin film deposited on top of it. However, the cracks were reported to be electrically reversible and reformed by switching the polarity of the electric field in PMN-PT(001) substrates by Liu *et al* [40]. Reversible crack modification has also been reported by Vinai *et al* in FeMn/PMN-PT(001) films, where out-of-plane polarization induced cracks in the film [41]. Upon reversing the applied electric field, the cracks were erased and a magnetically continuous film was generated.

In recent years, FeGa thin films have been studied in PMN-PT structures. FeGa alloys have a high magnetostriction constant, high tensile strength and soft magnetic behavior [42, 43]. The manipulation of magnetic hysteresis under the application of electric field has been shown by Phuoc *et al* [44, 45]. Ferromagnetic resonance studies have shown that the tailoring of resonant frequency and magnetic permeability can be done at different strained values [44, 46]. Some FeGa microstructures and nanostructures have been fabricated on PMN-PT substrates and the change in the local magnetic states by electric field in the presence of magnetic bias field has been realized [47, 48]. However, to the best of our knowledge, the characterization of domain textures in FeGa thin films on PMN-PT under the influence of electric field is missing in the literature.

Understanding the change of domain structures during magnetization reversal in the presence of electric fields is highly necessary to explain the effect of magnetoelectric coupling. In our work, we have performed detailed characterization of FeGa/PMN-PT heterostructures using magnetic domain analysis at each stage by correlating them with the hysteresis evolution and strain values. The realization of domain manipulation under various electric fields (different polarized PMN-PT states) gives insights about the coupling of magnetic domains with the ferroelectric domains of the PMN-PT. The as-deposited magnetic isotropic behavior of the sample was transformed into a magnetically anisotropic character under application of electric field, by exploiting the magneto-electric coupling effect. Using a Kerr microscope attached to the magneto-optic Kerr effect (MOKE) setup, the magnetic domains were recorded at all stages of the applied electric field to unveil the strain effects and the ferromagnetic–ferroelectric correlations. The magnetic anisotropy of the sample was modified and reproduced by cycling through various reversible strain states. The change of remanent magnetization of the sample was recorded by application of a cycling ON–OFF electric field process, through the use of a vibrating sample magnetometer (VSM). A completely non-volatile and reversible switching of magnetization was achieved.

2. Experimental methods

2.1. Sample preparation

$Fe_{70}Ga_{30}$ thin films were deposited on the polished side of (001) oriented $Pb(Mg_{1/3}Nb_{2/3})O_3$-$PbTiO_3$ (PMN-PT) substrates using sputtering at room temperature. The concentration of PT was between 30% and 34%. The thickness of the FeGa film was kept at 50 nm and 200 nm. The deposition was performed in the presence of an Ar environment. The pressure of the chamber during deposition was 1.1×10^{-2} mbar and the base pressure was at 10^{-7} mbar. No external magnetic field was applied during deposition. The substrates are 0.5 mm thick and have an Ag coating of 200–300 nm on the non-polished side. The substrates were purchased from MSE Supplies LLC (USA), which uses the Bridgman method for substrate preparation. The structured layer of FeGa on PMN-PT was observed with a scanning electron microscope (FEI Quanta3D-Inspect F).

2.2. Electric field application

The top and bottom surfaces of the FeGa/PMN-PT sample were contacted with a voltage source to generate out-of-plane electric fields as sketched in figure 1(a). To achieve this, the Ag coating on the back side of the sample is used as the bottom electrode and the top metallic surface made of the magnetic material is contacted to a Cu wire using Ag paste, making it as the top electrode. These top and bottom electrodes are connected to the voltage source present inside a Keithley 6517A Electrometer.

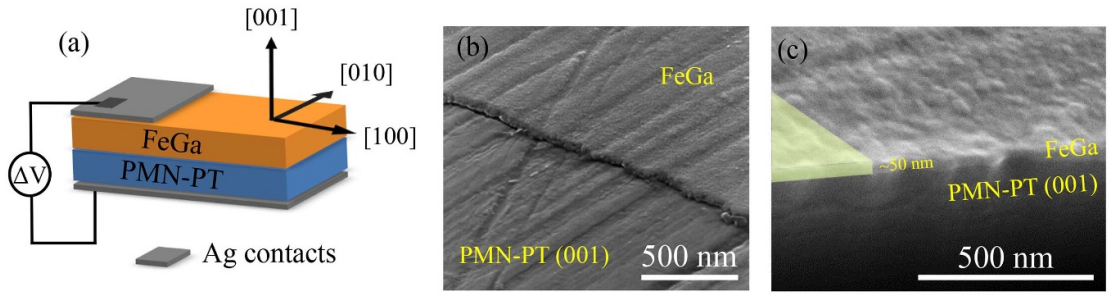

Figure 1. (a) Schematic of FeGa/PMN-PT heterostructure with Ag contacts as top and bottom electrodes for voltage application. (b, (c) The SEM images showing the thickness and cross-section at different magnification and tilt.

2.3. Strain calculation

In order to measure the in-plane strain generated in the sample, a strain gauge was attached to the top surface using Ag paste. The internal resistance and the *k*-factor of the strain gauge were 120 ± 0.35 ohms and 1.67, respectively. The two ends of the strain gauge were connected in a half-Wheatstone bridge setup with another reference strain gauge with the same specifications. The strain was measured using an HBM MGC plus strain acquisition system where the strain value was calibrated to a fixed resistance. The change in resistance of the strain gauge reflects the value of strain experienced and is measured in ppm.

2.4. Magnetic characterization methods

The magnetization reversal mechanism of the FeGa/PMN-PT samples was studied with the help of a MOKE based microscope by Evico magnetics. A magnification achieved by a 20× objective lens was sufficient to observe the large domains. The in-plane magnetic hysteresis loops were measured in the longitudinal mode at different voltages applied to the PMN-PT substrate. The corresponding magnetic domain images of the scanning area were recorded during reversal of magnetization. The remanent magnetization of the sample was also recorded as a function of time during ON–OFF voltage application by using a VSM, by Lakeshore Cryotronics, Inc., at zero magnetic field.

3. Results and discussion

Figure 1(b) reports an SEM image representing the deposited FeGa layer on PMN-PT. Here, the sample is observed under a 51° tilt to visualize the correlations of the surface of the FeGa layer with that of the PMN-PT. The cross section of the FeGa/PMN-PT stack was observed by etching with a focused ion beam, revealing the interface as shown in figure 1(c). The thickness of the FeGa layer is ~50 nm. A more precise calculation of the thickness was performed using an atomic force microscope (AFM). The granular morphology of FeGa is observed and the roughness of the film was calculated to be ~5 nm, which is similar to that of the PMN-PT surface. The magnetic film imitates the surface topography of the substrate. However, it is smooth and continuous throughout the sample. The magnetic hysteresis loops were measured using longitudinal MOKE for the as-deposited $Fe_{70}Ga_{30}$ (50 nm)/PMN-PT sample along the in-plane axes. The normalized hysteresis loops are shown in figure 2(a) along the [100], [110] and [010] axes by the red, green and orange curves, respectively. The shapes of the hysteresis curves are of squared type and are similar to each other, representing an isotropic in-plane behavior. These loops correspond to the illuminated area of the polarized light in the Kerr microscope and represent an intensity shift with changing magnetic field amplitude. The magnetic domain contrasts of the illuminated area were also recorded during the magnetization reversal, which are represented by figures 2(b)–(d). The images shown are recorded at the points marked by hysteresis loops (near the negative coercive field) to observe any domains forming during the reversal for all three axes separately. The bright and dark contrast regions point along the positive and negative field directions forming 180° domain walls. The reversal of magnetization is sharp and occurs via domain wall motion, also confirmed by the shape of the hysteresis loop.

The in-plane strain generated in the sample along the [100] direction is represented in figure 3, measured using a strain gauge adhered to the sample plane. A bipolar electric field was cycled with a maximum value of ±10 kV cm^{-1} applied perpendicular to the sample along the [001] direction. The strain has a linearly increasing response as the field is increased from −10 kV cm^{-1}. At nearly +2 kV cm^{-1}, it reaches its peak magnitude of 460 ppm and starts decreasing as the field is further increased. A similar response is observed as the field is decreased from +10 kV cm^{-1} where the strain reaches peak magnitude again at −2 kV cm^{-1}.

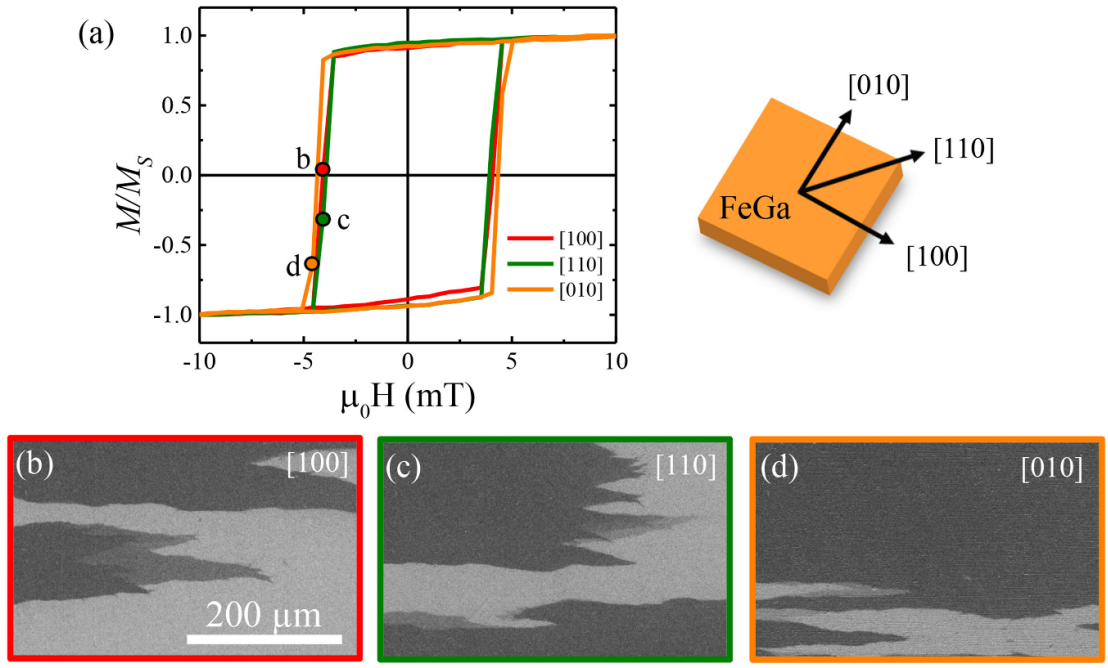

Figure 2. (a) Magnetic hysteresis curves of as-deposited $Fe_{70}Ga_{30}$ (50 nm)/PMN-PT along [100], [110] and [010] are shown by red, green and orange curves, respectively. The corresponding magnetic domain images during the magnetization reversal (points marked in the loops) along the three axes are shown in (b)–(d).

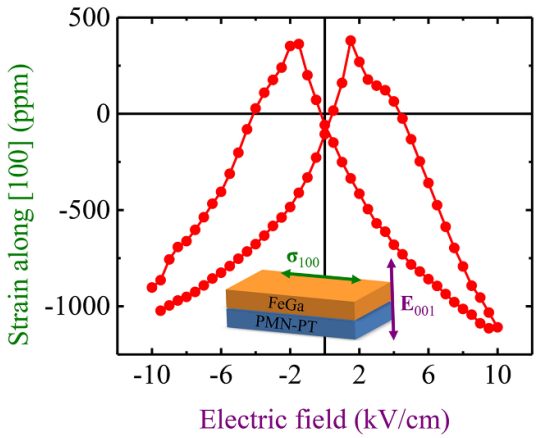

Figure 3. In-plane strain generated along the [100] direction as a function of electric field intensity applied along the [001] direction and cycled within ± 10 kV cm^{-1}.

At near saturation electric field values (± 10 kV cm^{-1}), the ferroelectric domains are aligned along the [001] and [00$\bar{1}$] directions (out-of-plane domains). This stretches the PMN-PT along the [001] direction, thereby generating compressive stress (negative strain) along the [100] and [010] directions. As the field magnitude is decreased and reversed to 2 kV cm^{-1}, the domains switch to in-plane configurations, stretching the material and generating positive strain along the in-plane directions. These mark the two coercive electric fields where the polarization of the PMN-PT switches. The strain responses are similar in behavior along both the [100] and [010] directions [38, 39].

After the strain measurement, the sample was kept at a positive remanent strained state (switching from $+10$ kV cm^{-1} to 0 kV cm^{-1}). The magnetic hysteresis loops and domain textures were studied at this remanent state to determine any change in magnetic anisotropy. Figure 4(a) shows the evolution of magnetic hysteresis loops recorded in longitudinal MOKE in different in-plane directions (measured angles are w.r.t. [100] direction). The area of the hysteresis curves decreases as the sample is rotated from the [100] axis towards the [010] axis, with the maximum achieved at 0° (red curve) and the minimum at 90° (orange curve). This confirms the generation of a magnetic anisotropy in the system with a preferential easy and hard

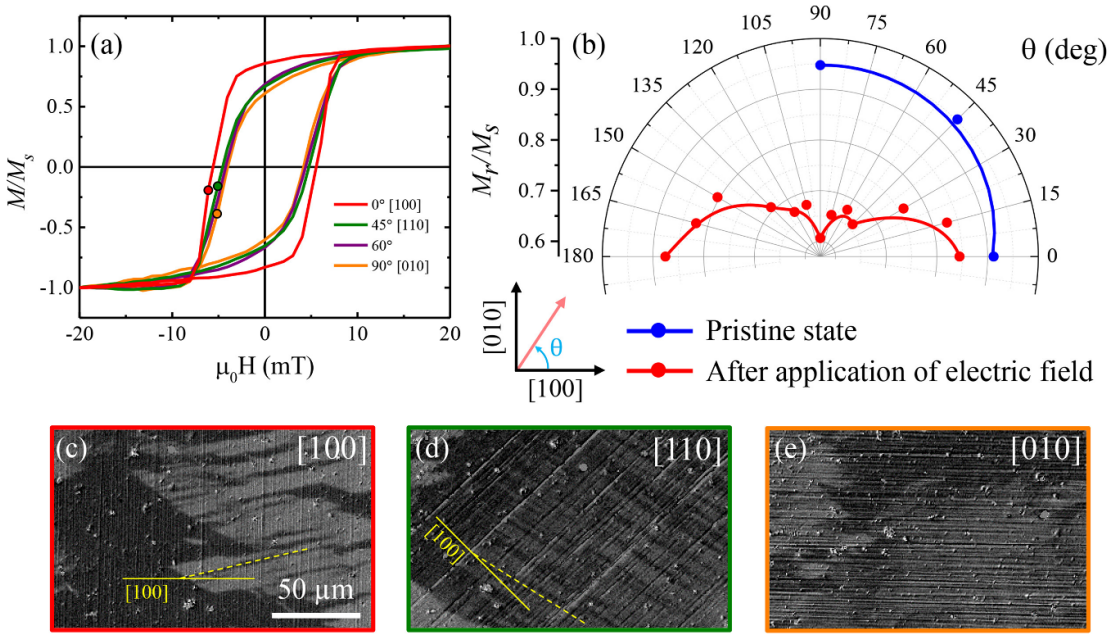

Figure 4. The evolution of magnetic hysteresis along different axes after application of electric field to the FeGa/PMN-PT sample is shown in (a). (b) Polar plot of magnetic remanence vs measured angle w.r.t [100] direction. The magnetic domain images during the magnetization reversal (recorded at points marked in the hysteresis loops) along [100], [110] and [010] are shown in (c)–(e), respectively.

axis in the system. The polar plot of normalized magnetic remanence (M_r/M_s) as a function of measured angle is shown in figure 4(b) by the red curve. This represents a nearly uniaxial anisotropy, where the magnetic remanence is reduced by 30% between the hysteresis recorded at 0° and 90° as compared to the isotropic behavior in the pristine state (blue curve). Magnetic domain patterns were also recorded during magnetization reversal. The near coercive field domain patterns (points marked in the loops) recorded along [100], [110] and [010] are represented in figures 4(c)–(e), respectively. In figure 4(c), the magnetic domains start to switch along the negative field direction, as represented by the darker contrasts creating 180° domain walls. The reversal of magnetization occurs via the formation of large domains and small magnetic stripes with subsequent domain wall motion. When the sample is rotated to 45°, more densely packed domains are formed, which are parallel to each other (figure 4(d)). The domains point along the same direction as seen in figure 4(c) (i.e. 13° w.r.t. [100] as marked by the yellow dotted lines). This shows a direct implication of the coupling of magnetic domains with the ferroelectric domains of the poled PMN-PT. Along the [010] direction (shown by figure 4(e)), the magnetization reversal is dominated by coherent rotation with small regions having faint domain contrasts. The easy axis in our sample is along 0° [100] due to the orientation of the nearly horizontal piezoelectric domains that generates horizontal magnetic domains (figure 4(c)). Alternatively, the hard axis points along 90° [010]. The inclusion of the magnetic anisotropy in the system after application of an electric field is directly associated with the magneto-electric coupling between the ferromagnetic domains with the newly aligned ferroelectric domains in the remanent state. The domains forming during the pristine state (figure 2) are very large as compared to the domains forming in the easy axis of the poled sample (figure 4(c)).

The application of voltage across the sample induced an instantaneous change in the original shape of the hysteresis loops and domain textures. In order to understand the effect at various strained states, the magnetic hysteresis curves were further recorded by applying a constant electric field during a hysteresis loop measurement. Figures 5(a) and (c) represent the hysteresis loops along the [100] and [010] directions at different electric field intensities. The green, orange and blue curves represent the longitudinal hysteresis loops measured at 10 kV cm^{-1}, 0 kV cm^{-1} and −2 kV cm^{-1} field intensities, respectively. With an application of 10 kV cm^{-1}, the area of the hysteresis loop decreased along [100] and increased along [010], indicating a rotation in the magnetic anisotropy of the system as compared to the remanent state in figure 4(a). The effect on the shape of hysteresis is hugely impacted by the negative strain (compressive stress) experienced at the interface by the FeGa layer with a high value of −1108 ppm (marked by the green dot in the strain curve in figure 5(b)). Meanwhile, the remanence of the hysteresis along the [010] axis increases due to a relatively lower compressive strain compared to [100] [39]. The magnetic domains

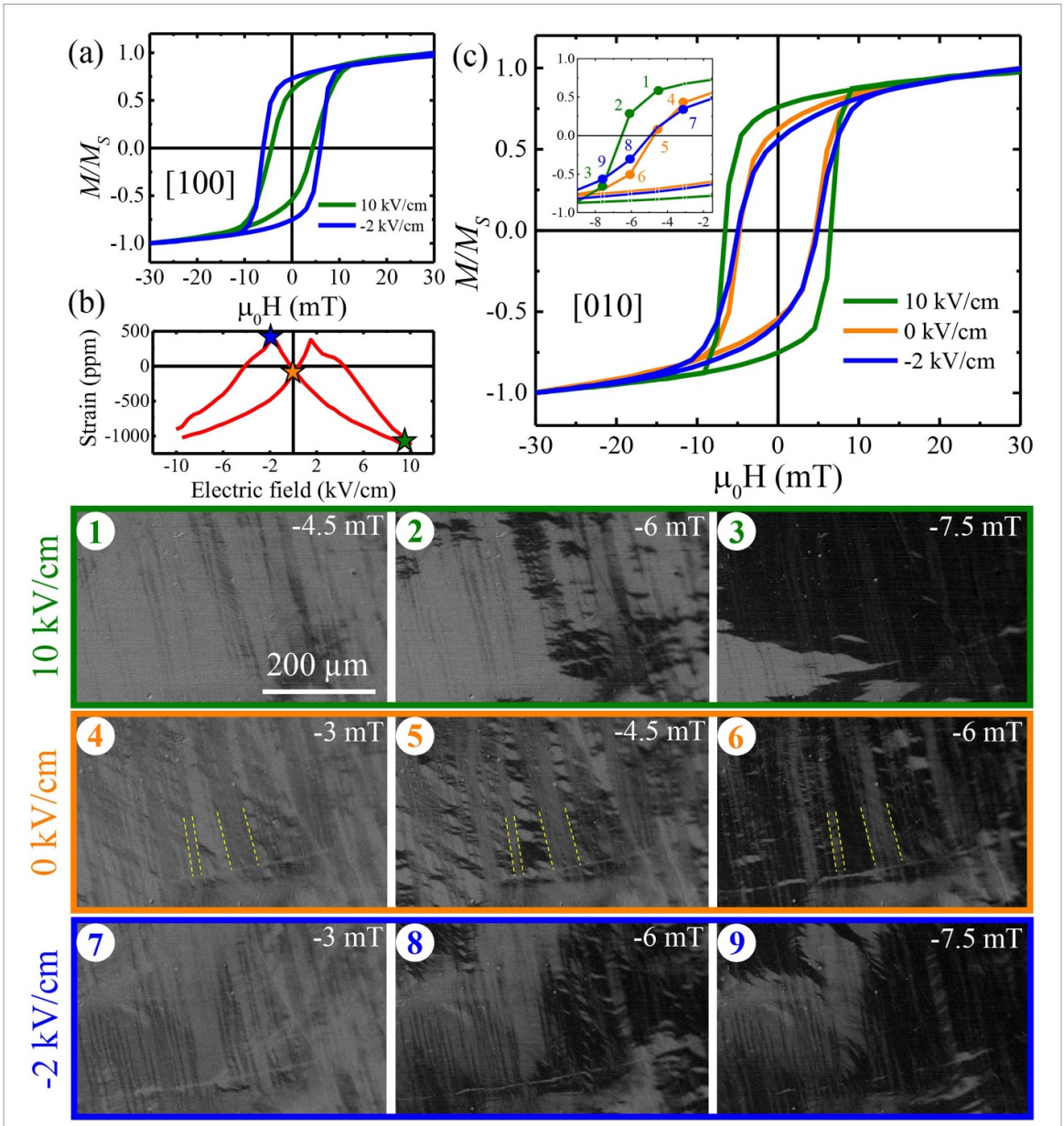

Figure 5. Magnetic hysteresis curves of FeGa/PMN-PT along the [100] and [010] directions (shown by (a) and (c), respectively) for different electric field intensities of 10 kV cm^{-1} (green), 0 kV cm^{-1} (orange) and −2 kV cm^{-1} (blue). The corresponding strain values are referenced in the strain curve (b). The domain structures recorded during magnetization reversal at these electric fields are shown by (c) 1–3, (c) 4–6 and (c) 7–9, respectively representing the points marked in the inset of (c).

recorded during the reversal along [010] show several nucleation sites (figure 5(c)2) and large domains as shown in figure 5(c)3. The reversal occurring is sharp and propagated by domain wall motions. As the electric field is reduced to 0 kV cm^{-1}, the shape of the hysteresis changed from a squared type to an S-shaped type with lower remanence and coercive field values as represented by the orange curve. The Kerr contrast during the magnetization reversal (figures 5(c)4–(c)6) reveals two different domain patterns. There is vertical segregation between different domains, one being a grey contrast indicating the coherent rotation and the other with dark–bright–dark domain contrasts involving domain wall propagation locally during reversal. This combination of two different domain types is due to correlations of the ferromagnetic domains with the possible vertical ferroelectric domains oriented along two different directions. The vertical segregation between the two different magnetic domain patterns varies between 10 and 50 μm (marked by the dotted yellow lines). These sizes are indeed similar to the reported sizes of ferroelectric domains in PMN-PT, which vary between 10 and 100 μm [49]. Similar domain correlations are reported in the case of CoFe/$BaTiO_3$ samples where magnetic stripes are coupled to a ferroelectric c-domain and a single magnetic domain with an a_1-domain [50]. As the field is brought to a positive strained state (at −2 kV cm^{-1}), the film is relaxed along the in-plane axes with in-plane ferroelectric domains in the PMN-PT. The magnetic

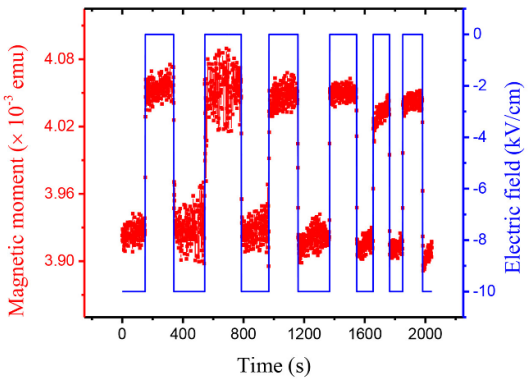

Figure 6. Switching of positive remanent magnetization (red curve) as an electric field of 10 kV cm^{-1} amplitude is kept in an ON–OFF process (blue curve).

hysteresis represented by the blue curve has even lower remanence. The domain structures are represented by figures 5(c)7–(c)9 where they are also impacted by the vertical segregation of different types similar to figure 5(c)5.

The magnetic moment of the $Fe_{70}Ga_{30}$ (50 nm)/PMN-PT sample was recorded with VSM to observe the change under application of electric field. However, due to the low thickness and small size of the sample, the magnitude of the recorded moment was low. In order to have higher magnetic moment response, a thicker sample with FeGa thickness of 200 nm was deposited on PMN-PT. The $Fe_{70}Ga_{30}$ (200 nm)/PMN-PT sample was measured to quantify the change in remanent magnetization as a function of electric field switching between the saturation (-10 kV cm^{-1}) and zero field values. The magnetization was recorded as a function of time with the field switching at an average interval of 200 s and the magnetic moment is recorded along the [100] direction as represented by the red curve in figure 6. The electric field switching is represented by the blue curve. The magnetization decreases as an electric field of -10 kV cm^{-1} is applied and the cycling magnetization has a stabilized change after a certain number of cycles. At 0 kV cm^{-1}, the sample relaxes to the remanent state with almost zero strain along the in-plane axes, which increases the net magnetic moment. However, at -10 kV cm^{-1}, the FeGa film experiences negative strain (compressive) along both in-plane axes which tries to align the magnetic moments along the out-of-plane direction, thereby decreasing the in-plane component of the magnetization.

4. Conclusion

The effect of electric field on the magnetization reversal of $Fe_{70}Ga_{30}$/PMN-PT(001) has been investigated. The application of electric field induced a significant magnetic anisotropy in an isotropic pristine system. This can be attributed to the local strain generated at the interface due to expansion and contraction of the PMN-PT substrate. Apart from the tensile and compressive stresses generated under different electric fields, the magnetic domains are also affected by the coupling with the underlying ferroelectric domains of the PMN-PT. This hugely impacts the modification of the magnetic hysteresis and thereby the magnetic anisotropy. The magnetic domain structures were significantly impacted at the saturation electric field of $+10$ kV cm^{-1} forming larger domains. At remanent strained states, the discrete magnetic domains were highly coupled with the relaxed ferroelectric domains, which lowers the anisotropy of the system. The domain contrasts recorded with MOKE and the normalized hysteresis curves represented a qualitative domain analysis. The measurements performed with VSM give more insight into the actual change of the net magnetic moment as the sample is placed under the application of electric field. Under an ON–OFF electric field application with a magnitude of 10 kV cm^{-1}, a cycling behavior of the magnetization was recorded. Our work reveals the possibility of manipulation of magnetization and domain structures with the application of electric field. These studies can be exploited for energy efficient electric field driven spintronics.

Data availability statement

All data that support the findings of this study are included within the article (and any supplementary files).

Acknowledgments

This work has received funding from the European Union's Horizon 2020 research and innovation programme under the Marie Skłodowska-Curie Grant Agreement No 861145. The experimental work has been partially performed at NanoFacility Piemonte, an INRIM laboratory supported by Compagnia di San Paolo.

ORCID iDs

Gajanan Pradhan https://orcid.org/0000-0001-5932-5211
Marco Coisson https://orcid.org/0000-0002-2978-7615
Gabriele Barrera https://orcid.org/0000-0002-3174-8092
Paola Rizzi https://orcid.org/0000-0002-3977-2839

References

[1] Åkerman J 2005 Toward a universal memory *Science* **308** 508–10
[2] Scott J 2007 Multiferroic memories *Nat. Mater.* **6** 256–7
[3] Bibes M and Barthélémy A 2008 Towards a magnetoelectric memory *Nat. Mater.* **7** 425–6
[4] Manipatruni S, Nikonov D E, Lin C-C, Gosavi T A, Liu H, Prasad B, Huang Y-L, Bonturim E, Ramesh R and Young I A 2019 Scalable energy-efficient magnetoelectric spin–orbit logic *Nature* **565** 35–42
[5] Leung C M, Li J, Viehland D and Zhuang X 2018 A review on applications of magnetoelectric composites: from heterostructural uncooled magnetic sensors, energy harvesters to highly efficient power converters *J. Phys. D: Appl. Phys.* **51** 263002
[6] Bibes M 2012 Nanoferronics is a winning combination *Nat. Mater.* **11** 354–7
[7] Spaldin N A and Ramesh R 2019 Advances in magnetoelectric multiferroics *Nat. Mater.* **18** 203–12
[8] Song C, Cui B, Li F, Zhou X and Pan F 2017 Recent progress in voltage control of magnetism: materials, mechanisms and performance *Prog. Mater. Sci.* **87** 33–82
[9] Hu J-M, Chen L-Q and Nan C-W 2016 Multiferroic heterostructures integrating ferroelectric and magnetic materials *Adv. Mater.* **28** 15–39
[10] Matsukura F, Tokura Y and Ohno H 2015 Control of magnetism by electric fields *Nat. Nanotechnol.* **10** 209–20
[11] Xiang Y *et al* 2020 Strain and phase transformation co-mediated magnetoelectric effect in epitaxial Ni/PMN-PT (011) heterostructures *J. Magn. Magn. Mater.* **514** 167138
[12] Hunt R G, Franke K J, Shepley P M and Moore T A 2023 Strain-coupled domains in $BaTiO_3$(111)–CoFeB heterostructures *Phys. Rev.* B **107** 014409
[13] Hill N A 2000 Why are there so few magnetic ferroelectrics? *J. Phys. Chem.* B **104** 6694–709
[14] Scott J F 2013 Room-temperature multiferroic magnetoelectrics *npg Asia Mater.* **5** e72–e72
[15] Lahtinen T H and van Dijken S 2013 Temperature control of local magnetic anisotropy in multiferroic CoFe/$BaTiO_3$ *Appl. Phys. Lett.* **102** 112406
[16] Ghidini M *et al* 2015 Perpendicular local magnetization under voltage control in Ni films on ferroelectric $BaTiO_3$ substrates *Adv. Mater.* **27** 1460–5
[17] Cherifi R *et al* 2014 Electric-field control of magnetic order above room temperature *Nat. Mater.* **13** 345–51
[18] Brivio S, Petti D, Bertacco R and Cezar J 2011 Electric field control of magnetic anisotropies and magnetic coercivity in Fe/$BaTiO_3$ (001) heterostructures *Appl. Phys. Lett.* **98** 092505
[19] Baldrati L, Rinaldi C, Manuzzi A, Asa M, Aballe L, Foerster M, Biškup N, Varela M, Cantoni M and Bertacco R 2016 Electrical switching of magnetization in the artificial multiferroic CoFe/$BaTiO_3$ *Adv. Electron. Mater.* **2** 1600085
[20] Radaelli G *et al* 2014 Electric control of magnetism at the Fe/$BaTiO_3$ interface *Nat. Commun.* **5** 3404
[21] Bauer U, Yao L, Tan A J, Agrawal P, Emori S, Tuller H L, Van Dijken S and Beach G S 2015 Magneto-ionic control of interfacial magnetism *Nat. Mater.* **14** 174–81
[22] Weisheit M, Fähler S, Marty A, Souche Y, Poinsignon C and Givord D 2007 Electric field-induced modification of magnetism in thin-film ferromagnets *Science* **315** 349–51
[23] Jeong J, Aetukuri N, Graf T, Schladt T D, Samant M G and Parkin S S 2013 Suppression of metal-insulator transition in VO_2 by electric field–induced oxygen vacancy formation *Science* **339** 1402–5
[24] Heidler J, Piamonteze C, Chopdekar R, Uribe-Laverde M A, Alberca A, Buzzi M, Uldry A, Delley B, Bernhard C and Nolting F 2015 Manipulating magnetism in $La_{0.7}Sr_{0.3}MnO_3$ via piezostrain *Phys. Rev.* B **91** 024406
[25] Yan H *et al* 2019 A piezoelectric, strain-controlled antiferromagnetic memory insensitive to magnetic fields *Nat. Nanotechnol.* **14** 131–6
[26] Zhi B, Gao G, Xu H, Chen F, Tan X, Chen P, Wang L and Wu W 2014 Electric-field-modulated nonvolatile resistance switching in VO_2/PMN-PT(111) heterostructures *ACS Appl. Mater. Interfaces* **6** 4603–8
[27] Bokov A and Ye Z-G 2006 Recent progress in relaxor ferroelectrics with perovskite structure *J. Mater. Sci.* **41** 31–52
[28] Noheda B, Cox D, Shirane G, Gao J and Ye Z-G 2002 Phase diagram of the ferroelectric relaxor (1-x)$PbMg_{1/3}Nb_{2/3}O_{3-x}PbTiO_3$ *Phys. Rev.* B **66** 054104
[29] Zhang Y, Xue D, Wu H, Ding X, Lookman T and Ren X 2014 Adaptive ferroelectric state at morphotropic phase boundary: coexisting tetragonal and rhombohedral phases *Acta Mater.* **71** 176–84
[30] Wang M *et al* 2020 Lateral electric-field-controlled perpendicular magnetic anisotropy and current-induced magnetization switching in multiferroic heterostructures *Adv. Electron. Mater.* **6** 2000229
[31] Leiva L, Torres J A, Gómez J, Rodriguez D V, Milano J and Butera A 2022 Electric field control of magnetism in FePt/PMN-PT heterostructures *J. Magn. Magn. Mater.* **544** 168619
[32] Guo X *et al* 2016 Electric field induced magnetic anisotropy transition from fourfold to twofold symmetry in (001) 0.68Pb$(Mg_{1/3}Nb_{2/3})O_3$-0.32$PbTiO_3$/$Fe_{0.86}Si_{0.14}$ epitaxial heterostructures *Appl. Phys. Lett.* **108** 152401

[33] Zhao X et al 2020 Shear-strain-induced over 90° rotation of local magnetization in FeCoSiB/PMN-PT (011) multiferroic heterostructures *Acta Mater.* **199** 495–503
[34] Wu T, Zhao P, Bao M, Bur A, Hockel J L, Wong K, Mohanchandra K P, Lynch C S and Carman G P 2011 Domain engineered switchable strain states in ferroelectric (011)[Pb ($Mg_{1/3}$ $Nb_{2/3}$)O_3](1 − x) -[$PbTiO_3$]$_x$ (PMN-PT, x≈0.32) single crystals *J. Appl. Phys.* **109** 124101
[35] Heidler J et al 2016 Magnetoelectroelastic control of magnetism in an artificial multiferroic *Phys. Rev.* B **94** 014401
[36] Buzzi M, Chopdekar R V, Hockel J L, Bur A, Wu T, Pilet N, Warnicke P, Carman G P, Heyderman L J and Nolting F 2013 Single domain spin manipulation by electric fields in strain coupled artificial multiferroic nanostructures *Phys. Rev. Lett.* **111** 027204
[37] Ghidini M et al 2018 Voltage control of magnetic single domains in Ni discs on ferroelectric $BaTiO_3$ *J. Phys. D: Appl. Phys.* **51** 224007
[38] Thiele C, Dörr K, Bilani O, Rödel J and Schultz L 2007 Influence of strain on the magnetization and magnetoelectric effect in $La_{0.7}$ $A_{0.3}$ MnO_3/PMN-OT(001)(A = Sr,Ca) *Phys. Rev.* B **75** 054408
[39] Ba Y et al 2018 Spatially resolved electric-field manipulation of magnetism for CoFeB mesoscopic discs on ferroelectrics *Adv. Funct. Mater.* **28** 1706448
[40] Liu Z et al 2018 Electrically reversible cracks in an intermetallic film controlled by an electric field *Nat. Commun.* **9** 41
[41] Vinai G et al 2019 Reversible modification of ferromagnetism through electrically controlled morphology *Adv. Electron. Mater.* **5** 1900150
[42] Atulasimha J and Flatau A B 2011 A review of magnetostrictive iron–gallium alloys *Smart Mater. Struct.* **20** 043001
[43] Pradhan G et al 2022 Magnetic properties of FeGa/Kapton for flexible electronics *Sci. Rep.* **12** 17503
[44] Phuoc N N and Ong C 2017 Electrical manipulation of electromagnetic properties of FeGa/[$Pb(Mg_{1/3}$ $Nb_{2/3})O_3]_{0.68}$−[$PbTiO_3]_{0.32}$(011) multiferroic heterostructures *J. Mater. Sci., Mater. Electron.* **28** 5628–33
[45] Begué A and Ciria M 2021 Strain-mediated giant magnetoelectric coupling in a crystalline multiferroic heterostructure *ACS Appl. Mater. Interfaces* **13** 6778–84
[46] Jiménez M J, Cabeza G, Gomez J E, Rodriguez D V, Leiva L, Milano J and Butera A 2020 Thickness dependence of the magnetoelectric coupling in $Fe_{89}Ga_{11}$ thin films deposited on ferroelectric PMN-PT single crystals *J. Magn. Magn. Mater.* **501** 166361
[47] De Jesus M G et al 2022 Magnetic state switching in fega microstructures *Smart Mater. Struct.* **31** 035005
[48] Ahmad H, Atulasimha J and Bandyopadhyay S 2015 Electric field control of magnetic states in isolated and dipole-coupled FeGa nanomagnets delineated on a PMN-PT substrate *Nanotechnology* **26** 401001
[49] Zhao E, Fang Z, Cheng M, Qin Y, Jiang X, Li X and Zhang Y 2020s In situ observation of two-step 90° domain reversal with different characteristics in PMN–38% PT single crystal *J. Mater. Sci.* **55** 8041–9
[50] Lahtinen T H, Franke K J and van Dijken S 2012 Electric-field control of magnetic domain wall motion and local magnetization reversal *Sci. Rep.* **2** 1–6